

Amorphous ZnO_xN_y thin films with high electron Hall mobility exceeding 200 cm² V⁻¹ s⁻¹

Takanori Yamazaki, Kei Shigematsu, Yasushi Hirose, Shoichiro Nakao, Isao Harayama, Daiichiro Sekiba, and Tetsuya Hasegawa

Citation: *Appl. Phys. Lett.* **109**, 262101 (2016); doi: 10.1063/1.4973203

View online: <http://dx.doi.org/10.1063/1.4973203>

View Table of Contents: <http://aip.scitation.org/toc/apl/109/26>

Published by the [American Institute of Physics](#)

Articles you may be interested in

[High mobility BaSnO₃ films and field effect transistors on non-perovskite MgO substrate](#)
Appl. Phys. Lett. **109**, 262102262102 (2016); 10.1063/1.4973205

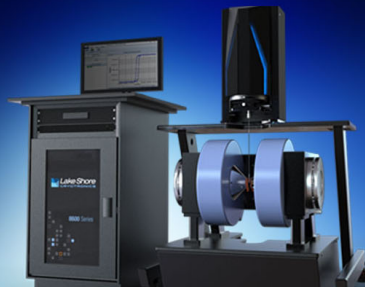
[Hybrid complementary circuits based on p-channel organic and n-channel metal oxide transistors with balanced carrier mobilities of up to 10 cm²/Vs](#)
Appl. Phys. Lett. **109**, 263301263301 (2016); 10.1063/1.4972988

[Densification of a-IGZO with low-temperature annealing for flexible electronics applications](#)
Appl. Phys. Lett. **110**, 011903011903 (2017); 10.1063/1.4973629

[High-performance PbS quantum dot vertical field-effect phototransistor using graphene as a transparent electrode](#)
Appl. Phys. Lett. **109**, 263101263101 (2016); 10.1063/1.4972984




Lake Shore
CRYOTRONICS



NEW 8600 Series VSM

For fast, highly sensitive
measurement performance

LEARN MORE 

Amorphous ZnO_xN_y thin films with high electron Hall mobility exceeding $200 \text{ cm}^2 \text{ V}^{-1} \text{ s}^{-1}$

Takanori Yamazaki,¹ Kei Shigematsu,² Yasushi Hirose,^{1,2,a)} Shoichiro Nakao,² Isao Harayama,³ Daiichiro Sekiba,^{3,4} and Tetsuya Hasegawa^{1,2}

¹Department of Chemistry, School of Science, The University of Tokyo, Bunkyo, Tokyo 113-0033, Japan

²Kanagawa Academy of Science and Technology (KAST), Kawasaki, Kanagawa 213-0012, Japan

³Graduate School of Pure and Applied Sciences, University of Tsukuba, 1-1-1 Tennoudai, Tsukuba, Ibaraki 305-8573, Japan

⁴University of Tsukuba Tandem Accelerator Complex (UTTAC), 1-1-1 Tennoudai, Tsukuba, Ibaraki 305-8577, Japan

(Received 2 October 2016; accepted 13 December 2016; published online 27 December 2016)

Zinc oxynitride (ZnO_xN_y) has attracted much attention as an amorphous semiconductor with high electron mobility. Recent studies reported that ZnO_xN_y thin films grown by sputtering contained nanocrystals, which might reduce their electron mobility through grain boundary scattering. In this study, we fabricated amorphous ZnO_xN_y thin films on a glass substrate by a less-energetic nitrogen-plasma-assisted pulsed laser deposition (PLD) to suppress the formation of the nanocrystals. Grown by PLD under optimized conditions, these ZnO_xN_y thin films exhibited extremely flat surfaces with a root-mean-squared roughness (R_{rms}) of less than 0.3 nm. The Hall mobility of these films exceeded $200 \text{ cm}^2 \text{ V}^{-1} \text{ s}^{-1}$ at a critical carrier concentration of $\sim 1 \times 10^{19} \text{ cm}^{-3}$, which was twice as high as the reported values for sputter-deposited films. Meanwhile, the mobility of films with larger R_{rms} was limited to $\sim 160 \text{ cm}^2 \text{ V}^{-1} \text{ s}^{-1}$ even at the critical carrier concentration and comparable with that of the sputter-deposited ZnO_xN_y films. The substantial enhancement in mobility in extremely flat ZnO_xN_y films demonstrated that suppressing the formation of nanocrystals is the key to fabricating amorphous ZnO_xN_y thin films with very high mobility. *Published by AIP Publishing.* [<http://dx.doi.org/10.1063/1.4973203>]

In the last decade, amorphous oxide semiconductors (AOSs) have been extensively studied because of their high electron mobility of over $10 \text{ cm}^2 \text{ V}^{-1} \text{ s}^{-1}$, which is one order of magnitude higher than those of the amorphous Si:H.^{1,2} Conventionally, AOSs are alloys of two or more metal oxides with different crystal structures where the metal has an electron configuration of $ns^0(n-1)d^{10}$ ($n \geq 4$), such as ZnO (wurtzite), Ga_2O_3 (β - Ga_2O_3), In_2O_3 (bixbyite), and SnO_2 (rutile). Because the conduction band minima (CBM) in these oxides consist of spatially spread and isotropic metal *s*-orbitals, electron transfer in AOSs is robust against structural distortion, allowing for a high electron mobility even in the amorphous phases.

Recently, Ye *et al.* proposed a mixed anion compound, zinc oxynitride (ZnO_xN_y), as a novel amorphous semiconductor.³ In contrast to the conventional AOSs, amorphous ZnO_xN_y is an alloy of an oxide (ZnO, wurtzite) and a nitride (Zn_3N_2 , anti-bixbyite) that have the same cation. A remarkable feature of amorphous ZnO_xN_y is its high electron Hall mobility, over $100 \text{ cm}^2 \text{ V}^{-1} \text{ s}^{-1}$,⁴⁻⁶ which is comparable with the highest reported values for AOSs.^{7,8} However, more recent studies using transmission electron microscopy (TEM) and electron diffraction revealed that these “amorphous” ZnO_xN_y thin films contained nanocrystals of ZnO and Zn_3N_2 ,⁴ which would reduce their mobility through grain boundary scattering. Conversely, the mobility of amorphous ZnO_xN_y thin films can be further enhanced by reducing the nanocrystals.

To suppress the formation of nanocrystals in this paper, we focused on the deposition process. In the previous studies,³⁻⁶ ZnO_xN_y thin films were fabricated by reactive sputtering. However, sputtering frequently causes unintentional substrate heating^{9,10} and collisions of high-energy particles with the film surface during deposition, which would induce crystallization of the film.^{11,12} In this study, we fabricated ZnO_xN_y thin films by using nitrogen-plasma-assisted pulsed laser deposition (NPA-PLD), in which the above-mentioned “heating” effects are less significant because of lower averaged power of the ablation laser (typically less than 1 W). The ZnO_xN_y thin films grown under optimized conditions exhibited very flat surfaces owing to the suppression of nanocrystals and twice as high electron Hall mobility, $240 \text{ cm}^2 \text{ V}^{-1} \text{ s}^{-1}$, as that of the reported sputter-deposited films.

The ZnO_xN_y thin films were grown by NPA-PLD¹³⁻¹⁶ on alkali-free glass substrates (Corning, EagleXG) without heating the substrate. The substrate temperature during deposition was $< 50^\circ\text{C}$, measured using a nonreversible temperature indicator (Nichiyu Giken Kogyo, Thermo Label). A ceramic ZnO target (99.999%) was ablated by a KrF excimer laser with a target-to-substrate distance of 50 mm. The laser energy fluence was set to $\sim 0.2 \text{ J cm}^{-2}$ per pulse, nearly the ablation threshold, to minimize the kinetic energy of the ablated species.¹⁷ Indeed, the films grown at a high laser energy fluence tended to crystallize. The typical deposition rate and thickness of the films *t* were 0.4–0.7 nm/min and ~ 30 nm, respectively. Nitrogen radicals were supplied from an electron cyclotron resonance (ECR) plasma source (Tectra, Gen2

^{a)}Author to whom correspondence should be addressed. Electronic mail: hirose@chem.s.u-tokyo.ac.jp

Atomsource). The partial pressure of N_2 gas introduced into the growth chamber was fixed at 5×10^{-5} Torr, and the amount of nitrogen radicals was controlled by the input current of the ECR source (I_{ECR}). The background pressure of the growth chamber was lower than 3×10^{-9} Torr.

The crystal structure and surface morphology of the ZnO_xN_y films were evaluated by X-ray diffraction (XRD; Bruker AXS, D8 DISCOVER with GADDS) and atomic force microscopy (AFM; SII, SPI4000 with SPA400), respectively. The chemical compositions of the films were determined by elastic recoil detection analysis (ERDA) for N and O as well as the Rutherford backscattering spectrometry (RBS) for Zn with a 38.4 MeV ^{35}Cl beam generated by a 5-MV tandem accelerator (Micro Analysis Laboratory, The University of Tokyo [MALT]).¹⁸ To reduce the background oxygen from the substrate, ZnO_xN_y films deposited on Si substrate were used for the ERDA measurement. The ratio of effective solid angles of the detectors for ERDA and RBS measurements was calibrated using a stoichiometric ZnO thin film. The experimental errors in the x and y values were determined by statistical errors, and were less than $\pm 5\%$ under a typical condition (total dose of $\sim 2 \times 10^{12}$ ions). The optical transmittance T and reflectance R of the films were measured by using a UV/visible/near-infrared spectrophotometer (JASCO, V-670). The absorption coefficient α was calculated by $T/(1-R) = \exp(-\alpha \cdot t)$. The electrical resistivity (ρ), carrier density (N_c), and Hall mobility (μ) of the films were measured at room temperature using the six-probe method with the standard Hall bar geometry.

Figure 1 shows the chemical compositions of the ZnO_xN_y thin films deposited with various I_{ECR} . For the ZnO_xN_y films grown with $I_{\text{ECR}} \leq 15$ mA, the nitrogen amount y monotonically increased with increasing I_{ECR} . The nominal charges of Zn, evaluated as $2x + 3y$, in these films were smaller than +2, suggesting the existence of metal Zn as an impurity phase. However, for $I_{\text{ECR}} \geq \sim 15$ mA, y is saturated and the chemical composition was almost constant as $ZnO_{0.31}N_{0.46}$. The nominal charges of Zn calculated from this composition was nearly +2, indicating the disappearance of

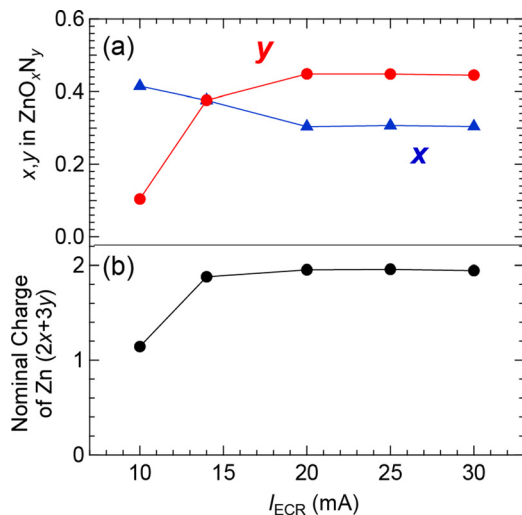


FIG. 1. (a) Chemical compositions of the ZnO_xN_y thin films fabricated with various I_{ECR} . (b) Nominal charge of Zn in the ZnO_xN_y thin films ($2x + 3y$) calculated from the x and y values in (a) plotted against I_{ECR} .

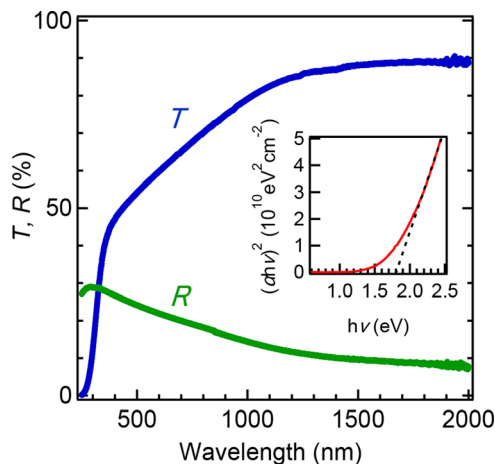


FIG. 2. Optical transmittance (T) and reflectance (R) spectra of the $ZnO_{0.31}N_{0.46}$ thin film fabricated with $I_{\text{ECR}} = 30$ mA. Inset shows the $(\alpha h\nu)^2 - h\nu$ plot (direct transition model) of the film.

metal Zn. Hereafter, we focused on the films grown with $I_{\text{ECR}} \geq \sim 15$ mA to prevent the presence of metal Zn from influencing the physical properties. Figure 2 shows the optical properties of the $ZnO_{0.31}N_{0.46}$ thin film fabricated with $I_{\text{ECR}} = 30$ mA. Using the Tauc plot assuming a direct transition— $(\alpha h\nu)^2$ vs. $h\nu$, where h and ν represent the Planck's constant and the frequency of incident light, respectively—we evaluated the absorption edge of the film to be ~ 1.8 eV. This value is very different from those of ZnO and Zn_3N_2 , indicating that the film consisted of a single-phase ZnO_xN_y , not a mixture of ZnO and Zn_3N_2 . Although Zn_3N_2 thin films containing interstitial nitrogen may show a similar optical gap,^{19,20} this possibility can be eliminated from the results of XRD and Hall measurements, as described below.

Figure 3 shows $\theta-2\theta$ XRD patterns of the ZnO_xN_y thin films fabricated with various I_{ECR} . All of the films exhibited featureless patterns without any diffraction peaks. Despite the similarity in the XRD patterns, these ZnO_xN_y thin films had very different surface morphologies that strongly depended on I_{ECR} , as follows. The ZnO_xN_y films fabricated with low I_{ECR} exhibited a grain-like surface structure (Figs.

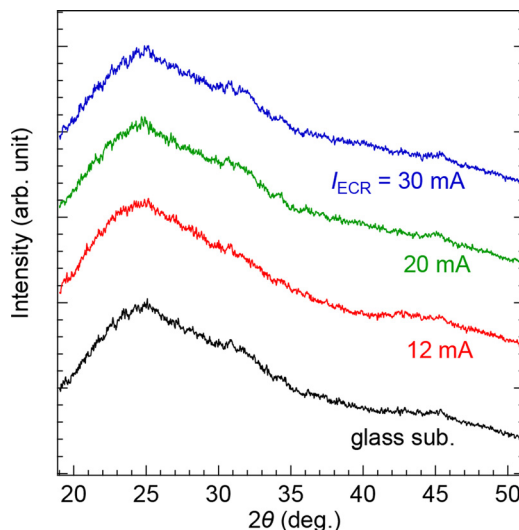


FIG. 3. $\theta-2\theta$ XRD patterns of the ZnO_xN_y thin films fabricated with various I_{ECR} .

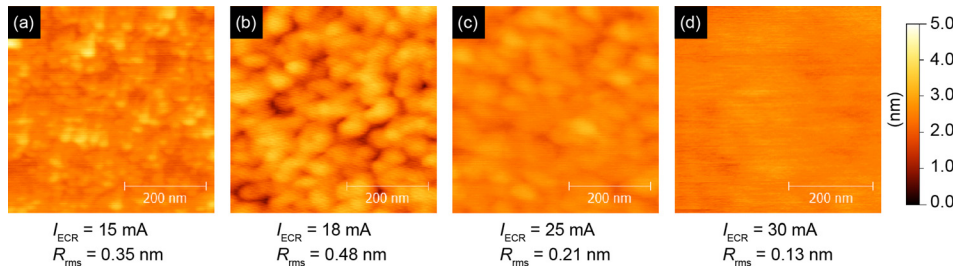


FIG. 4. AFM images ($0.5 \times 0.5 \mu\text{m}^2$) of the ZnO_xN_y thin films fabricated with I_{ECR} = (a) 15 mA, (b) 18 mA, (c) 25 mA, and (d) 30 mA. Also shown are R_{rms} values calculated from the AFM images.

4(a) and 4(b)). Because a similar grain-like structure appeared for the sputter-deposited films containing nanocrystals,⁵ we believe that these structures originated from nanocrystals inside the films. In contrast, the ZnO_xN_y films fabricated with high I_{ECR} showed a smoother surface without a grain-like structure, and the root-mean-squared surface roughness (R_{rms}) reached the same level as the glass substrates, ~ 0.2 nm (Fig. 4(d)). Because such an extremely flat surface is a characteristic feature of amorphous oxide thin films grown by PLD,^{21,22} we reasonably conclude that the decrease of surface roughness comes from the reduction of nanocrystals. For simplicity, we hereafter classified our films into two groups based on R_{rms} : films containing nanocrystals ($R_{\text{rms}} \geq 0.3$ nm) and supposedly “completely” amorphous films without nanocrystals ($R_{\text{rms}} < 0.3$ nm).

Figures 5(a)–5(c) plot the N_e , μ , and R_{rms} of the ZnO_xN_y thin films as functions of I_{ECR} , respectively. As shown in Figs. 5(a) and 5(b), as I_{ECR} increased, N_e decreased, and μ increased. Notably, the μ of the ZnO_xN_y thin films fabricated with $I_{\text{ECR}} \geq 25$ mA exceeded $200 \text{ cm}^2 \text{ V}^{-1} \text{ s}^{-1}$, which is even higher than those of the polycrystalline ZnO (Ref. 23) and Zn_3N_2 (Refs. 19 and 20) thin films. The carrier (electron) source of the ZnO_xN_y thin films are probably anion vacancies as in the cases of AOSs.²¹ In order to verify this assignment, a small amount of oxygen gas (partial pressure $P_{\text{O}_2} \leq 5 \times 10^{-6}$ Torr) was introduced during the deposition with a constant $I_{\text{ECR}} = 30$ mA. As shown in Fig. 5(d), N_e monotonically decreased with an increasing P_{O_2} , supporting that anion vacancies are the dominant source of carrier electrons. It was also observed that the introduction of oxygen gas induces an increase of R_{rms} and a reduction of μ (Figs. 5(e) and 5(f)), while the change of anion composition was smaller than the experimental error in compositional analysis. Figure 5(g) summarizes μ – R_{rms} relation of the ZnO_xN_y thin films. Although the plots are scattered probably due to the influence of N_e , as discussed later, they can be obviously classified into two groups below and above a critical R_{rms} of ~ 0.3 nm: All of the “completely” amorphous films showed μ higher than $170 \text{ cm}^2 \text{ V}^{-1} \text{ s}^{-1}$, while μ in the other films were at most $\sim 160 \text{ cm}^2 \text{ V}^{-1} \text{ s}^{-1}$ and were in almost the same range as the reported data for the sputter-deposited ZnO_xN_y thin films^{3–5} (shaded area in Fig. 5(g)). This difference in μ between these two groups supports the scenario that the increased μ is attributable to a reduction in grain-boundary scattering.

Another possible factor for enhancement of μ is the carrier density N_e . Figure 6 showed the relation between μ and N_e of the PLD-grown ZnO_xN_y thin films together with the literature values for sputter-deposited ones.^{3,5} The PLD-grown films containing nanocrystals (triangles) showed a peak μ at

N_e of $\sim 1 \times 10^{19} \text{ cm}^{-3}$, indicating a change in the dominant carrier transport mechanism at this critical N_e as reported in amorphous oxide semiconductors.^{21,24} A similar peak of μ was observed for the sputter-deposited ZnO_xN_y although we have to take into account the influence of the chemical compositions on μ .⁴ the PLD-grown films have a constant anion composition of $\text{N}/(\text{N}+\text{O}) \sim 0.6$ whereas the sputter-deposited films showed a wide variety of chemical composition⁵ (Fig. 6, inset). We also admit that the N_e values of the “completely” amorphous ZnO_xN_y thin films (circles) are close to the critical N_e ($\sim 1 \times 10^{19} \text{ cm}^{-3}$), indicating that the closeness of N_e to the critical value is one of the origins of their very high μ . On the other hand, the shape of the μ – N_e curve strongly suggests the presence of another origin for the

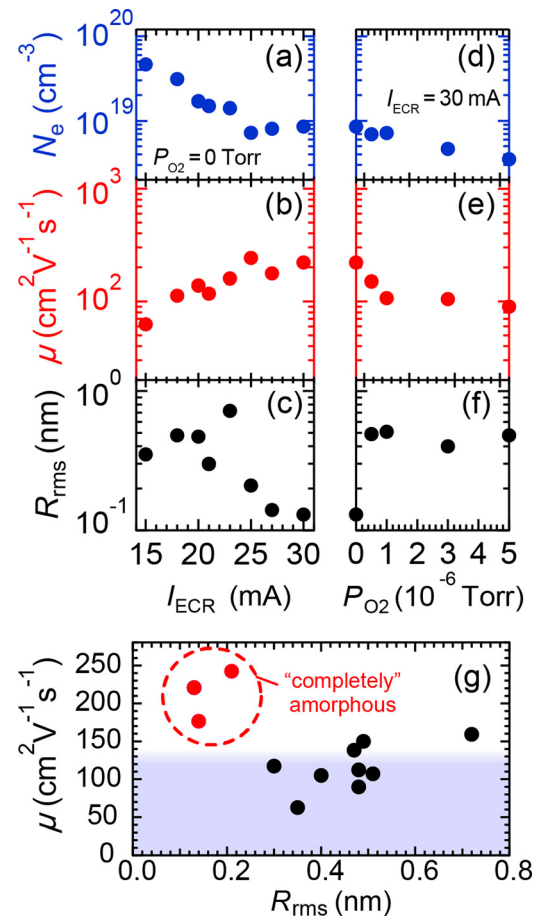


FIG. 5. ((a), (d)) Carrier density N_e , ((b), (e)) Hall mobility μ , and ((c), (f)) surface roughness R_{rms} of ZnO_xN_y thin films. ((a)–(c)) Properties of the films fabricated with various I_{ECR} without O_2 introduction and ((d)–(f)) those with constant $I_{\text{ECR}} = 30$ mA and various P_{O_2} . R_{rms} values were calculated from the AFM images over $0.5 \times 0.5 \mu\text{m}^2$. (g) Hall mobility of the ZnO_xN_y thin films plotted against R_{rms} . Shaded area represents the mobility range reported for sputter-deposited ZnO_xN_y thin films.^{3–5}

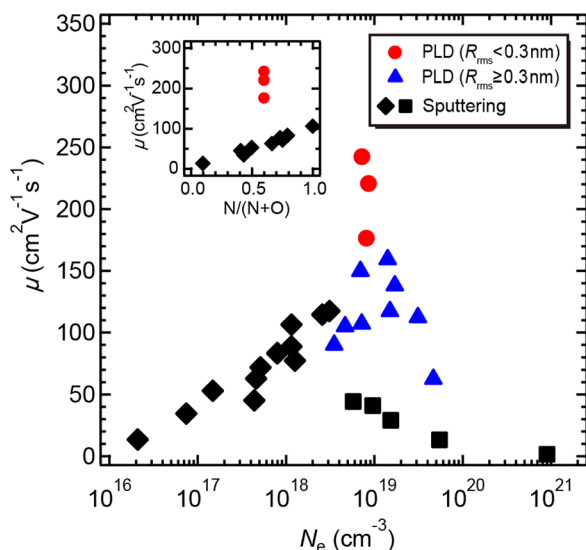


FIG. 6. Hall mobility of the ZnO_xN_y thin films plotted against carrier density. Circles and triangles are values from the PLD-grown films with $R_{\text{rms}} < 0.3$ nm (“completely” amorphous) and from those with $R_{\text{rms}} \geq 0.3$ nm (containing nanocrystals), respectively. The squares (Ref. 3) and diamonds (Ref. 5) are values for reported sputter-deposited films. Inset shows the mobilities of the “completely amorphous” films grown by PLD and those of the sputter-deposited films (Ref. 5) as a function of the anion composition.

mobility enhancement in these films: It is generally known that the $\mu-N_e$ curves of oxide semiconductors have a broad peak at the critical N_e . Indeed, the $\mu-N_e$ curves of the ZnO_xN_y films containing nanocrystals show a broad peak. In contrast, μ of the “completely” amorphous ZnO_xN_y thin films shows a very sharp peak, which is significantly distinguished from the broad peak feature described above. Therefore, we believe that the substantial enhancement in μ from ~ 160 $\text{cm}^2 \text{V}^{-1} \text{s}^{-1}$ to ~ 250 $\text{cm}^2 \text{V}^{-1} \text{s}^{-1}$ at the critical N_e in the “completely” amorphous ZnO_xN_y films is attributable to a reduction of nanocrystals.

In summary, we fabricated the “completely” amorphous ZnO_xN_y thin films on glass substrates by NPA-PLD. The closeness of N_e to a critical value and the suppressed formation of nanocrystals dramatically enhanced μ in the ZnO_xN_y thin films up to >200 $\text{cm}^2 \text{V}^{-1} \text{s}^{-1}$, which is twice as high as those of the sputter-deposited ZnO_xN_y thin films. These results demonstrate that less-energetic deposition is the key to fabricating amorphous ZnO_xN_y thin films with a very high μ . It is also suggested that a high μ around 200 $\text{cm}^2 \text{V}^{-1} \text{s}^{-1}$ can be achieved even in sputter-deposited ZnO_xN_y thin films by preventing the formation of nanocrystals. Facing-target sputtering¹² and/or heavier noble gas sputtering (Kr or Xe)

might be effective in preventing the unintentional substrate heating and/or the formation of high-energy charged particles.

We thank Professor Hiroyuki Matsuzaki of The University of Tokyo for his assistance in ERDA measurements. This study was financially supported by CREST, Japan Science and Technology Agency (JST) and Tokyo Ohka Foundation for The Promotion of Science and Technology.

- ¹K. Nomura, H. Ohta, A. Takagi, T. Kamiya, M. Hirano, and H. Hosono, *Nature* **432**, 488 (2004).
- ²T. Kamiya, K. Nomura, and H. Hosono, *Sci. Technol. Adv. Mater.* **11**, 044305 (2010).
- ³Y. Ye, R. Lim, and J. M. White, *J. Appl. Phys.* **106**, 074512 (2009).
- ⁴E. Lee, A. Benayad, T. Shin, H. Lee, D.-S. Ko, T. S. Kim, K. S. Son, M. Ryu, S. Jeon, and G.-S. Park, *Sci. Rep.* **4**, 4948 (2014).
- ⁵H.-S. Kim, S. H. Jeon, J. S. Park, T. S. Kim, K. S. Son, J.-B. Seon, S.-J. Seo, S.-J. Kim, E. Lee, J. G. Chung, H. Lee, S. Han, M. Ryu, S. Y. Lee, and K. Kim, *Sci. Rep.* **3**, 1459 (2013).
- ⁶E. Lee, T. Kim, A. Benayad, J. Hur, G.-S. Park, and S. Jeon, *Sci. Rep.* **6**, 23940 (2016).
- ⁷E. Fortunato, P. Barquinha, A. Pimentel, L. Pereira, G. Goncalves, and R. Martins, *Phys. Status Solidi RRL* **1**, R34 (2007).
- ⁸M.-G. Kim, H. S. Kim, Y.-G. Ha, J. He, M. G. Kanatzidis, A. Facchetti, and T. J. Marks, *J. Am. Chem. Soc.* **132**, 10352 (2010).
- ⁹V. I. Shapovalov, A. E. Komlev, A. S. Bondarenko, P. B. Baykov, and V. V. Karzin, *Phys. Lett. A* **380**, 882 (2016).
- ¹⁰J. A. Thornton, *Thin Solid Films* **54**, 23 (1978).
- ¹¹I. Brodie, L. T. Lamont, Jr., and D. O. Myers, *J. Vac. Sci. Technol.* **6**, 124 (1969).
- ¹²K. Ellmer and T. Welzel, *J. Mater. Res.* **27**, 765 (2012).
- ¹³D. Oka, Y. Hirose, H. Kamisaka, T. Fukumura, K. Sasa, S. Ishii, H. Matsuzaki, Y. Sato, Y. Ikuhara, and T. Hasegawa, *Sci. Rep.* **4**, 4987 (2014).
- ¹⁴D. Oka, Y. Hirose, T. Fukumura, and T. Hasegawa, *Cryst. Growth Des.* **14**, 87 (2014).
- ¹⁵A. Suzuki, Y. Hirose, D. Oka, S. Nakao, T. Fukumura, S. Ishii, K. Sasa, H. Matsuzaki, and T. Hasegawa, *Chem. Mater.* **26**, 976 (2014).
- ¹⁶J. Takahashi, Y. Hirose, D. Oka, S. Nakao, C. Yang, T. Fukumura, I. Harayama, D. Sekiba, and T. Hasegawa, *Appl. Phys. Lett.* **107**, 231906 (2015).
- ¹⁷R. E. Leuchtner, *Appl. Surf. Sci.* **127–129**, 626 (1998).
- ¹⁸I. Harayama, K. Nagashima, Y. Hirose, H. Matsuzaki, and D. Sekiba, *Nucl. Instrum. Methods Phys. Res., Sect. B* **384**, 61 (2016).
- ¹⁹X. Cao, A. Sato, Y. Ninomiya, and N. Yamada, *J. Phys. Chem. C* **119**, 5327 (2015).
- ²⁰T. Suda and K. Kakishita, *J. Appl. Phys.* **99**, 076101 (2006).
- ²¹K. Nomura, A. Takagi, T. Kamiya, H. Ohta, M. Hirano, and H. Hosono, *Jpn. J. Appl. Phys., Part 1* **45**, 4303 (2006).
- ²²S. Nakao, Y. Hirose, T. Fukumura, and T. Hasegawa, *Jpn. J. Appl. Phys., Part 1* **53**, 05FX04 (2014).
- ²³K. Ellmer, *J. Phys. D: Appl. Phys.* **34**, 3097 (2001).
- ²⁴A. J. Leenheer, J. D. Perkins, M. F. A. M. van Hest, J. J. Berry, R. P. O’Hayre, and D. S. Ginley, *Phys. Rev. B* **77**, 115215 (2008).